

# Reconciling STEM and X-ray Scattering Data To Determine the Nanoscale Ionic Aggregate Morphology in Sulfonated Polystyrene Ionomers

Nancy C. Zhou,<sup>†,§</sup> Christopher D. Chan,<sup>†</sup> and Karen I. Winey<sup>\*,†,‡</sup>

Department of Chemical and Biomolecular Engineering, University of Pennsylvania, Philadelphia, Pennsylvania 19104-6393, and Department of Materials Science and Engineering, University of Pennsylvania, Philadelphia, Pennsylvania 19104-6272

Received April 10, 2008; Revised Manuscript Received June 18, 2008

**ABSTRACT:** This paper reports the first quantitative reconciliation of imaging and scattering data for poly(styrene-*ran*-styrenesulfonate) (P(S-SS<sub>x</sub>)) ionomers. We examined the morphology of solvent-cast and spin-cast P(S-SS<sub>0.019</sub>)-M ionomers using the combination of scanning transmission electron microscopy (STEM) and X-ray scattering, where the scattering data were fit with a liquidlike hard-sphere model. Both the ionic aggregate sizes ( $R_1$ ) and the sample volume per ionic aggregate ( $V_p$ ) as measured by both techniques were in good agreement. In addition, STEM found that P(S-SS<sub>0.019</sub>) ionomers prepared by spin-casting exhibit nanometer spherical ionic aggregates that are indistinguishable in size, shape, and spatial distribution from the bulk solvent-cast ionomers. Six P(S-SS<sub>0.019</sub>)-M ionomers fully neutralized with various cations have ionic aggregate compositions that are predominately ionic, and the ionic aggregate radius ( $R_1$ ) increases as the cation radii increases. Finally, the influence of copolymer type was studied by comparing P(S-SS<sub>0.070</sub>) and P(S-MAA<sub>0.072</sub>) ionomers. The ionic aggregates in P(S-SS<sub>0.070</sub>)-Cu are surrounded by a thicker region of limited mobility and are more ionic as compared with P(S-MAA<sub>0.072</sub>) ionomers. Although STEM and X-ray scattering have been reconciled for these P(S-SS<sub>x</sub>) ionomers, a broad application of the liquidlike hard-sphere scattering model is not recommended. However, when STEM and X-ray scattering are reconciled, detailed morphological information can be extracted from the scattering data, particularly regarding the composition of the ionic aggregates, which is important for understanding the mechanisms of ion transport.

## Introduction

The field of ion-containing random copolymers has attracted much attention and research in recent decades. The inherent electrostatic forces drive microphase separation of the ionic groups into nanometer-sized ionic aggregates. These ionic aggregates facilitate ion transport and function as physical cross-links giving rise to their unique properties. These properties make possible a wide range of commercial applications for ionomers, including tough thermoplastics, adhesives, fuel cell membranes, and ion exchange resins.<sup>1–3</sup>

To advance the understanding of ionomer morphologies, our group applies scanning transmission electron microscopy (STEM) to various random and periodic ionomers. Our most noteworthy contribution to date involves the study of a poly(styrene-*ran*-methacrylic acid) (P(S-MAA<sub>x</sub>)) copolymer fully neutralized with divalent copper. We initially studied a model system of monodisperse gold nanoparticles (Au<sub>11</sub>) supported on polystyrene films varying in thickness (20–90 nm) to establish that results from our STEM techniques are in agreement with X-ray scattering fitted with an appropriate X-ray model.<sup>4</sup> The radius of the gold nanoparticle was measured by fitting a Gaussian to the intensity profile across the feature in the STEM image, which allowed for quick and reproducible measurements. A simple form-factor scattering model could be used to interpret the X-ray data because the gold nanoparticles were dilute, monodisperse hard spheres. The nanoparticle diameter determined by STEM imaging ( $D_{STEM}$ ) and X-ray scattering ( $2R_1$ ) are in quantitative agreement, thereby demonstrating that our STEM methods can

be used to image nanoscale objects in the presence of an amorphous polymer.

Our group next applied these STEM methods to examine the nanoscale morphology of a fully neutralized ionomer, P(S-MAA<sub>0.072</sub>)-Cu.<sup>5</sup> The sizes of the ionic aggregates were measured from the STEM images using the method just described, and the scattering data were fit with a liquidlike hard-sphere scattering model. The agreement was excellent, and we reported the first quantitative reconciliation of STEM images and X-ray scattering for the size of the spherical ionic aggregates in ionomers. The reconciliation of the number density of ionic aggregates ( $1/V_p$ ) proved more challenging and required image simulations to correct for the extensive overlap in the STEM images.<sup>6</sup> The liquidlike hard-sphere scattering model has a fitting parameter that is the inverse of the number density of ionic aggregates or the average sample volume per ionic aggregate ( $V_p$ ). (Note that  $V_p$  is not the volume of an ionic aggregate.) Using the fitting parameters from the liquidlike X-ray scattering model, the ionomer morphology was simulated in real space coordinates (3D) and then projected to form an intensity map (2D image). The detectable features in the projected images represented only a fraction of the total number of aggregates in the 3D volume. After accounting for this overlap effect and measuring the specimen thickness using electron energy loss spectroscopy (EELS),  $V_p$  calculated from STEM images was found to be consistent with the scattering data interpreted by the liquidlike model.

In contrast, our studies of poly(styrene-*ran*-styrenesulfonate) (P(S-SS<sub>x</sub>)) ionomers have presented inconsistent morphological descriptions via STEM and X-ray scattering.<sup>7,8</sup> Using STEM, a partially (25%) zinc-neutralized sulfonated polystyrene ionomer exhibited a heterogeneous distribution of Zn-rich aggregates, with some micron-sized regions exhibiting no aggregates and other regions possessing many aggregates. For neutralization

\* To whom correspondence should be addressed. E-mail: winey@seas.upenn.edu.

<sup>†</sup> Department of Chemical and Biomolecular Engineering.

<sup>‡</sup> Department of Materials Science and Engineering.

<sup>§</sup> IBM, 1000 River Street, Essex Junction, VT 05452.

levels greater than 75%, the Zn-rich aggregates were found to exhibit both spherical and vesicular shapes. However, the X-ray scattering data were readily fit with a model that assumes monodisperse spheres with liquidlike order. Obviously, these conflicting morphological observations indicate that neither STEM nor X-ray scattering can be used in isolation to reliably determine the size, shape, and spatial distribution of ionic aggregates in ionomers.

Previous studies of P(S-SS<sub>x</sub>) ionomers have found that sample preparation impacts the nanoscale morphology. For example, Weiss et al. showed changes in the X-ray scattering patterns when P(S-SS<sub>0.076</sub>)-Mn was cast from solvents of increasing polarity.<sup>9</sup> O'Connell et al. also demonstrated that the polarity of the casting solvent has significant effects on the morphology of P(S-SS<sub>0.017</sub>)-Na using Na-NMR.<sup>10</sup> Our interest is in spin-cast films of ionomers because we have prepared bilayer samples using this method to study the blend miscibility of P(S-SS<sub>0.007</sub>) ionomer systems.<sup>11,24</sup> The interpretation of our blend miscibility studies requires knowing the ionomer morphology, specifically the state of ionic aggregation.

While sample preparation affects the morphology of ionomers, the choice of neutralizing cation may also influence the ionic aggregate morphology. A X-ray scattering study of P(S-SS<sub>0.0691</sub>) neutralized with Rb (monovalent) or P(S-SS<sub>0.0691</sub>)-Sr (divalent) and interpreted with a liquidlike hard-sphere scattering model found that the ionic aggregate sizes depend only weakly on the cation.<sup>12</sup> In addition, Fitzgerald and Weiss found that the position of the ionomer peak of P(S-SS<sub>0.049</sub>) was unaffected by changing the cation for alkali metal salts, but the peak shifted to higher angle for divalent alkaline earth metal and transition metal salts.<sup>13</sup> To date, a detailed quantitative examination on a series of cations of varying valency and ionic radii has not yet been compiled in P(S-SS<sub>x</sub>) ionomers.

The quantitative agreement of direct imaging via STEM and X-ray scattering of both the ionic aggregate size ( $R_1$ ) and aggregate number density ( $1/V_P$ ) for P(S-MAA<sub>0.072</sub>)-Cu motivates our investigation of the ionomer morphology in other styrene-based ionomers. The P(S-SS<sub>x</sub>) ionomers are of particular interest due to their commercial importance and their difference in acid type and position of the acid group relative to P(S-MAA<sub>x</sub>) ionomers. Specifically, this paper examines the nanoscale morphology of solvent-cast P(S-SS<sub>0.019</sub>) ionomers neutralized with various cations. We report quantitative agreement with respect to the ionic aggregate size ( $R_1$ ) and aggregate number density ( $1/V_P$ ) as determined from STEM and X-ray scattering results. The morphologies of spun-cast ionomers are also presented, and the ionic aggregate sizes from STEM are comparable to the solution-cast ionomers. In addition, the morphologies of P(S-SS<sub>0.019</sub>)-M ionomers as a function of cations (M = Cu, Mg, Zn, Na, Ba, and Cs) are presented, and we report an increase in aggregate size with increasing cation size. Finally, we compare the ionic aggregates in P(S-SS<sub>x</sub>)-Cu and P(S-MAA<sub>x</sub>)-Cu ionomers.

## Experimental Section

**Materials.** Atactic polystyrene was purchased from Pressure Chemical ( $M_w = 65\,000$  g/mol, PDI = 1.06). Poly(styrene-*ran*-styrenesulfonate) copolymers P(S-SS<sub>x</sub>) were prepared according to the sulfonation procedure described in our previous paper.<sup>11</sup> The acetyl sulfate reaction at low substitutions yields nominally random monomeric sequences.<sup>14</sup> The acid mole fraction ( $x$ ) was determined by Robertson Microlit Analysis (Madison, NJ) using elemental sulfur analysis via ion chromatography. P(S-SS<sub>0.019</sub>) was converted to ionomer by first dissolving the copolymer in a mixture of toluene/methanol (90/10 v/v). A stoichiometric amount (125%) of dehydrated metal acetate salt was dissolved in 50/50 v/v toluene/methanol and added dropwise to the agitated P(S-SS<sub>x</sub>) solution. The combined solution was stirred for 1 h at ~40 °C. The

neutralized polymer was recovered by solvent-casting the solution at room temperature for 2 days and then dried under vacuum for 12 h at 115 °C. The resulting ionomers were delicate films and stored in a vacuum desiccator until examined. The metal cations are denoted by M in P(S-SS<sub>x</sub>)-M.

**X-ray Scattering.** For X-ray scattering, the P(S-SS<sub>0.019</sub>) solvent-cast and dried ionomers were melt-pressed at 160 °C and 15 000 psi for 5 min and then slowly cooled to room temperature. The X-ray scattering apparatus consists of a Nonius FR591 rotating-anode generator operated at 40 kV × 85 mA, mirror-monochromator focusing optics, an evacuated flight path, and a Bruker HiSTAR multiwire two-dimensional detector. Data were collected over 1 h intervals at a sample-detector distance of 54 cm.

The scattering data from P(S-SS<sub>0.019</sub>) ionomers were adjusted for background scattering by subtracting the scattering from an empty sample holder and azimuthally integrated to provide  $I$  vs  $q$ . The P(S-SS<sub>0.019</sub>) ionomer data were then fitted with liquidlike hard-sphere scattering model proposed by Kinning and Thomas<sup>15</sup>

$$I_{\text{KT}}(q) = A\Phi^2(qR_1) \frac{1}{1 + 24\eta\left(\frac{G(B)}{B}\right)} \quad (1)$$

where

$$\Phi(x) = 3 \frac{\sin x - x \cos x}{x^3} \quad (2)$$

$$\eta = \frac{4}{3}\pi R_{\text{CA}}^3 \frac{1}{V_P} \quad (3)$$

$$B = 2qR_{\text{CA}} \quad (4)$$

and

$$G(B) = \frac{(1 + 2\eta)^2}{B^2(1 - \eta)^4} (\sin B - B \cos B) - \frac{6\eta\left(1 + \frac{\eta}{2}\right)^2}{B^3(1 - \eta)^4} [2B \sin B + (2 - B^2) \cos B - 2] + \frac{\eta(1 + 2\eta)^2}{2B^5(1 - \eta)^4} \{-B^4 \cos B + 4[(3B^2 - 6) \cos B + (B^3 - 6B) \sin B + 6]\} \quad (5)$$

where  $A$  is peak amplitude,  $R_1$  is the radius of the ionic aggregate,  $R_{\text{CA}}$  is the radius of closest approach between two aggregates, and  $V_P$  is the sample polymer volume per ionic aggregate. This model incorporates the Percus-Yevick correlation function which includes the interference between all of hard spheres in the system as a radial density function from a central particle. This Kinning-Thomas model has four independent fitting parameters:  $A$ ,  $R_1$ ,  $R_{\text{CA}}$ , and  $V_P$ . A least-squares regression applied to generate a best fit model shown as a solid curve plotted along with the scattering data. A comparison between the liquidlike hard-sphere X-ray scattering model proposed by Yarusso and Cooper and the modified version that uses the Percus-Yevick correlation function proposed by Kinning and Thomas is included in the Supporting Information. 2D data reduction, analysis, and curve fitting were performed using Datasqueeze software.<sup>16</sup>

**Specimen Preparation and STEM.** STEM specimens were sectioned from the same bulk P(S-SS<sub>x</sub>)-M ionomers characterized by X-ray scattering. They were prepared using a Reichert-Jung ultramicrotome with a diamond knife at room temperature with a cutting speed of 0.4 mm/s and a nominal section thickness of 30 nm.

For comparison, the solution-cast P(S-SS<sub>0.019</sub>)-M ionomer films were dissolved in 80/20 (v/v) toluene/THF solution and spin-cast (2000 rpm, 60 s) from 1 wt % solutions onto clean Si substrates. The films were then annealed under vacuum for 12 h at 115 °C, after which the film thicknesses were measured by ellipsometry. The spin-cast films were floated onto ultrafiltered distilled water, collected onto Cu TEM grids, and dried under vacuum at room temperature.

STEM experiments were performed on a JEOL 2010F field emission electron microscope. The instrument was operated at 197

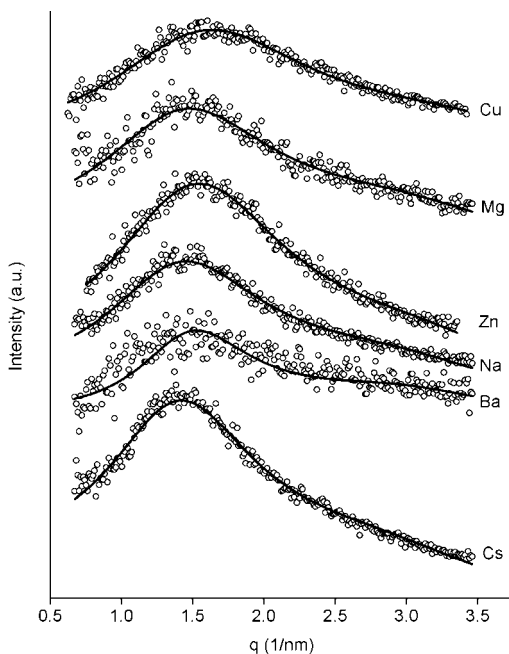


**Figure 1.** X-ray scattering intensity vs scattering angle for a series of solvent-cast P(S-SS<sub>0.019</sub>)-M ionomers fully neutralized with different cations (M). The data are shifted in arbitrary units to help differentiate the different X-ray results and are arranged with increasing ionic radii from Cu (smallest) to Cs (largest). Curves through the data are the best fit to the liquidlike hard-sphere scattering model, eq 1.

kV with a 0.7 nm STEM probe and a 70  $\mu\text{m}$  condenser aperture. Images were acquired using a high angle annular dark field (HAADF) scintillating detector with linear intensity response and collection angles of 50–110 mrad.

The contrast in HAADF-STEM images of P(S-SS<sub>0.019</sub>) ionomers arises from the atomic number differences, such that the brighter regions correspond to projections of higher average atomic number (Cu, Zn, Cs, or Ba rich domains). The size of an ionic aggregate is determined by fitting the intensity profile from across an isolated feature with a Gaussian curve. The average ionic aggregate size is the mean of  $\sim 35$  measurements.

**Modeling and Simulations.** The simulation constructs a 3D model of the ionomer morphology based on a user-defined volume and the parameters from the liquidlike hard-sphere scattering model ( $R_1$ ,  $R_{CA}$ ,  $V_P$ ). The volume with periodic boundary conditions is filled sequentially with hard spheres. From this 3D simulated morphology, a 2D intensity map is constructed to form a simulated STEM image. The details of this simulation were presented previously.<sup>6</sup> In this paper, we simulated a 50 nm  $\times$  50 nm  $\times$  thickness (10–100 nm) volume, constructed a 50 nm  $\times$  50 nm projection, and report the average number of features ( $N_{2D}$ ) from five projections.

## Results

**X-ray Scattering.** Figure 1 shows the X-ray scattering data of P(S-SS<sub>0.019</sub>) ionomers where the neutralizing cations consist of alkali (Na<sup>+</sup>, Cs<sup>+</sup>), alkaline (Mg<sup>2+</sup>, Ba<sup>2+</sup>), and transition metals (Zn<sup>2+</sup>, Cu<sup>2+</sup>). These six ionomers were solution-neutralized, followed by solvent-casting, drying, and compression-molding. The intensity of the X-ray scattering as a function of scattering vector ( $q$ ) shows a distinct ionomer peak at  $q \sim 1.5 \text{ nm}^{-1}$ , where the position of the ionomer peak is nominally constant for all six P(S-SS<sub>0.019</sub>) ionomers. The Kinning–Thomas model is in good agreement with the scattering data for all of the solvent-cast P(S-SS<sub>0.019</sub>) ionomers, and the fitting parameters ( $R_1$ ,  $R_{CA}$ ,  $V_P$ ) are reported in Table 1. Thus, the scattering results are consistent with morphologies containing uniformly distributed aggregates that are monodisperse and spherical.

**Scanning Transmission Electron Microscopy.** Figure 2 displays HAADF-STEM images of solvent-cast P(S-SS<sub>0.019</sub>)-Zn and P(S-SS<sub>0.019</sub>)-Ba ionomers. The ionic aggregates in these images appear monodisperse, spherical, and evenly distributed throughout the specimen. The features in the images of solvent-cast P(S-SS<sub>0.019</sub>)-Zn and P(S-SS<sub>0.019</sub>)-Ba ionomers have average diameters of  $1.6 \pm 0.4$  and  $1.2 \pm 0.3$  nm, respectively. The diameters from the X-ray fitting parameters were 1.4 nm in both systems. Therefore, the average diameters measured from the STEM image ( $D_{\text{STEM}}$ ) and the aggregate sizes from the X-ray scattering model ( $2R_1$ ) are in good agreement (Table 1).

Figure 3 shows the STEM images of P(S-SS<sub>0.019</sub>)-Zn and P(S-SS<sub>0.019</sub>)-Ba prepared by spin-casting the ionomer from solution. These images show that the ionic aggregates in spin-cast P(S-SS<sub>0.019</sub>)-Zn and P(S-SS<sub>0.019</sub>)-Ba samples also appear monodisperse, spherical, and evenly distributed throughout the specimen. The features in the images of P(S-SS<sub>0.019</sub>)-Zn and P(S-SS<sub>0.019</sub>)-Ba have average diameters of  $1.3 \pm 0.4$  and  $1.4 \pm 0.3$  nm. These sizes are indistinguishable from those found when these solution-neutralized ionomers were solvent-cast. Two additional spin-cast P(S-SS<sub>0.019</sub>) ionomers having high atomic number cations (Cs and Cu) were also examined by STEM, and their  $D_{\text{STEM}}$  are shown in Table 1. Within the experimental uncertainty of  $D_{\text{STEM}}$ , the ionic aggregates are the same size in these spun-cast thin films as they are in bulk samples when measured by STEM or X-ray scattering.

**Simulation of STEM Images.** Previously, Benetatos et al. examined P(S-MAA<sub>0.072</sub>)-Cu and found that the assumption of a one-to-one correspondence between the number of features observed in a 2D STEM image ( $N_{2D}$ ) and the number of ionic aggregates in a specimen volume ( $N_{3D}$ ) is inaccurate.<sup>6</sup> Rather, there is a severe overlap effect such that each individual feature in the STEM images (Figures 2 and 3) does not originate from a single aggregate, but from a number of highly overlapped aggregates. Interestingly, the extensive overlap produces projected 2D features that are comparable in size to the 3D particles, so that  $D_{\text{STEM}} \approx 2R_1$ .<sup>4</sup> In order to account for the overlap, we use a computer model to estimate the ratio of the number of observable 2D features in projection,  $N_{2D}$ , to the number of 3D particles in the volume,  $N_{3D}$ . From these simulations, we obtain the relationship between  $N_{2D}$  and  $N_{3D}$  as a function of sample thickness,  $t$ , for each ionomer:  $N_{3D} = N_{2D}t^x$ . Using the fitting parameters from the X-ray model ( $R_1$ ,  $R_{CA}$ ,  $V_P$ ), the  $x$  for each ionomer was found: 0.74, 0.77, 0.87, and 0.83 for Ba, Cs, Cu, and Zn, respectively.

To determine the  $V_P$  from STEM data ( $V_{P,\text{STEM}}$ ), we account for the extensive overlap by counting the distinct features in the STEM images ( $N_{2D,\text{STEM}}$ ), measuring the specimen thickness ( $t$ ), and applying  $N_{3D} = N_{2D,\text{STEM}}t^x$  from the simulations, as follows:

$$V_{P,\text{STEM}} = \frac{\text{Area}t}{N_{3D}} = \frac{\text{Area}t}{N_{2D}t^x} \quad (6)$$

where Area is the area of the image used to measure  $N_{2D,\text{STEM}}$ . Benetatos et al. applied electron energy loss spectroscopy (EELS) to microtomed specimens to determine specimen thickness.<sup>6</sup> Here, the thicknesses of the spin-cast films are measured by ellipsometry, which is both faster and more accurate than EELS. The resulting  $V_{P,\text{STEM}}$  from the spin-cast P(S-SS<sub>0.019</sub>) ionomers are given in Table 1 along with the estimated error which arises primarily from the determination of  $N_{2D,\text{STEM}}/\text{Area}$ . The  $V_P$  values as determined by the STEM imaging and the X-ray scattering data fit with the liquidlike model of hard spheres agree within measurement error of the two methods.

**Table 1. Morphology of Ionic Aggregates in Fully Neutralized P(S-SS<sub>0.019</sub>)-M Ionomers As Determined by X-ray Scattering and STEM**

	Zn	Ba	Cs	Cu	Na	Mg
solvent-cast, scattering model						
$2R_1$ (nm)	1.4	1.4	1.7	1.1	1.4	1.3
$2R_{CA}$ (nm)	3.6	3.9	3.9	3.2	3.8	3.7
$V_P$ (nm <sup>3</sup> )	174 ± 3	138 ± 9	199 ± 4	147 ± 5	204 ± 4	212 ± 6
solvent-cast, STEM results						
$D_{STEM}$ (nm)	1.6 ± 0.4	1.2 ± 0.3				
spin-cast, STEM results						
$D_{STEM}$ (nm)	1.3 ± 0.4	1.4 ± 0.3	1.3 ± 0.5	1.3 ± 0.4		
$V_{P,STEM}$ (nm <sup>3</sup> )	240 ± 83	164 ± 75	226 ± 52	195 ± 88		

## Discussion

**Reconciling STEM and X-ray Scattering.** STEM images are consistent with a liquidlike packing of monodisperse, spherical ionic aggregates in solvent-cast P(S-SS<sub>0.019</sub>) ionomers. This observation justifies the use of the model proposed by Kinning and Thomas to interpret the X-ray scattering data. The sizes of the Zn-, Ba-, Cs-, and Cu-rich ionic aggregates as determined by STEM ( $D_{STEM}$ ) and X-ray scattering ( $2R_1$ ) are in good agreement (Table 1). The number density of these ionic aggregates ( $1/V_P$ ) is also consistent between the two morphology characterization methods (Table 1).

These findings extend the work of Benetatos et al., where the authors reconciled STEM imaging and X-ray scattering for a P(S-MAA<sub>0.072</sub>)-Cu ionomer.<sup>6</sup> Our STEM results on poly(dimethylsiloxane) ionomers<sup>17</sup> and precipitated P(S-MAA) ionomers<sup>18</sup> show nonspherical morphologies; thus, the liquidlike scattering model cannot be universally applied.

The qualitative information from STEM is invaluable in establishing a reliable X-ray scattering model. In our opinion, this validation procedure is necessary prior to applying the Kinning–Thomas model to other ionomer systems or ionomers prepared differently. A validated X-ray scattering model has a number of advantages relative to STEM imaging: speed, sample

volume tested, and simplicity of extracting morphology parameters ( $R_1$  and  $V_P$ ). Thus, we rely on the numerical values from the verified X-ray scattering model to describe the morphology of these P(S-SS<sub>x</sub>) ionomers.

**Effect of Sample Preparation.** Both our solution-casting and spin-casting methods produce uniformly distributed, monodisperse and spherical ionic aggregates as interpreted from the STEM images. The size of the ionic aggregates determined by X-ray scattering from the solvent-cast sample and by STEM imaging from both solvent-cast and spin-cast samples are in good agreement. The volume per ionic aggregate determined by X-ray scattering from the solvent-cast sample and by STEM imaging from the spin-cast samples are also in good agreement. The data indicate that the morphologies prepared by slow solvent-casting and rapid spin-casting are qualitatively and quantitatively indistinguishable.

This finding is interesting given that earlier work has found significant variations in ionomer morphology with processing methods that alter the solvent removal rate. For example, Kirkmeyer et al. observed spatial heterogeneity in rapidly precipitated P(S-SS)-Zn samples.<sup>8</sup> Benetatos et al. used STEM to probe P(S-MAA<sub>0.072</sub>)-Cu and found that the rapidly precipi-

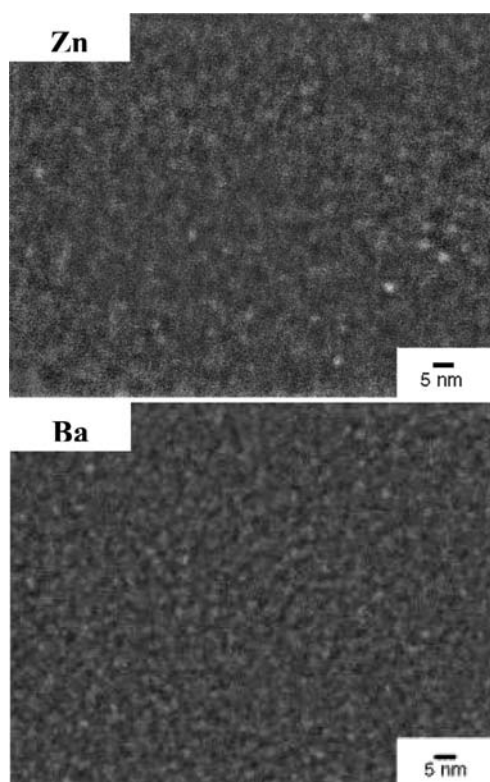


**Figure 2.** HAADF–STEM images of solvent-cast P(S-SS<sub>0.019</sub>)-Zn and P(S-SS<sub>0.019</sub>)-Ba ionomers show monodisperse, spherical ionic aggregates with uniform spatial distribution. The bright features represent extensive overlap of the high atomic number Zn- or Ba-rich aggregates.

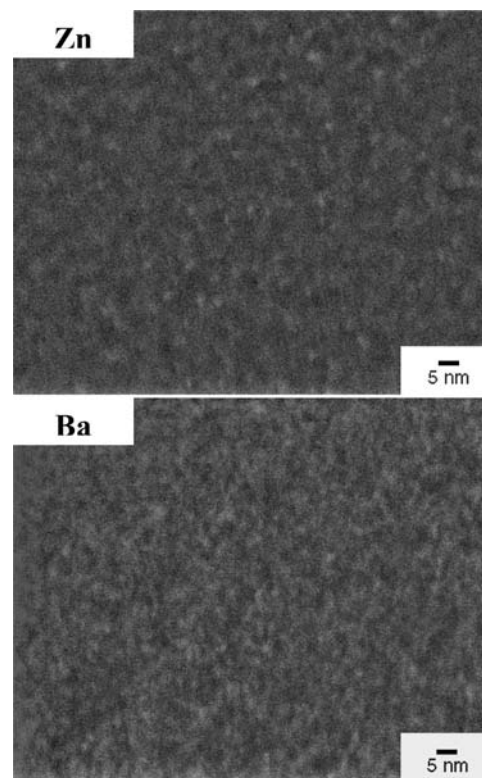


**Figure 3.** HAADF–STEM images of P(S-SS<sub>0.019</sub>)-Zn and P(S-SS<sub>0.019</sub>)-Ba ionomers prepared by spin-casting thin films. The thickness of each sample is 50 nm as determined by ellipsometry. The bright features correspond to monodisperse, spherical Zn- or Ba-rich ionic aggregates.

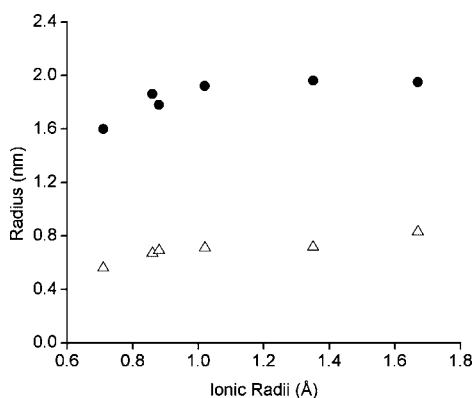


**Figure 4.** Radius of the cation-rich ionic aggregate,  $R_1$  (△), and the radius of closest approach,  $R_{CA}$  (●), as obtained from fitting X-ray scattering data with eq 1 are plotted against the ionic radii of the neutralizing cations. Cation radii increase from  $\text{Cu}^{2+}$ ,  $\text{Mg}^{2+}$ ,  $\text{Zn}^{2+}$ ,  $\text{Na}^+$ ,  $\text{Ba}^{2+}$ , to  $\text{Cs}^+$ .

tated sample exhibited an irregular distribution of copper, while the slowly solvent-cast sample exhibited uniformly distributed spherical ionic aggregates.<sup>17</sup> Upon annealing, the morphology of these precipitated ionomers became indistinguishable from the solvent-cast materials. Note that the bulk materials and spin-cast films in this study were both subjected to annealing (115 °C, 12 h), which apparently explains their equivalent morphologies. Given the variety of processing methods available to P(S-SS<sub>x</sub>) ionomers, including steam stripping, solvent-casting, or precipitating after sulfonation or neutralization,<sup>19–21</sup> more investigations are necessary to fully understand the correlations between processing and morphology and then morphology and properties.

The spin-cast samples are of particular interest to us because we used this method of preparation in our previous blend miscibility studies.<sup>22,24</sup> In that study, homopolymer–ionomer blends of deuterated polystyrene (dPS) and P(S-SS<sub>0.007</sub>)-M show less miscibility and a higher upper critical solution temperature than the corresponding homopolymer–copolymer blends of dPS and P(S-SS<sub>0.007</sub>). Furthermore, the homopolymer–ionomer blends neutralized with divalent cations are less miscible than those neutralized with monovalent cations.

Our finding that the P(S-SS<sub>x</sub>)-M ionomer samples prepared by solvent-cast and spin-cast methods are indistinguishable has a number of ramifications. First, this critical observation implies that our miscibility studies in thin films are applicable to bulk materials. Second, the conclusion that solvent-cast bulk samples and spin-cast thin films of ionomers have equivalent morphologies opens the possibility of simpler STEM specimen preparation. In particular, spin-cast films can be prepared with well-defined thicknesses that are measured accurately ( $\pm 0.2\%$ ) by ellipsometry as compared to the laborious efforts to microtome thin sections from a bulk sample and then measure its thickness using the less accurate method of EELS ( $\pm 20\%$ ). Spin-casting will make STEM studies of ion-containing polymers easier. Third, thin films of ionomers can be probed by in situ microscopy methods to explore their response to temperature and electric fields.

**Ionic Aggregate Size and Composition.** Having verified the liquidlike scattering model for these ionomers, we now use the fitting parameters from the model to investigate the morphology of the ionic aggregates as a function of cation type. The X-ray scattering data in Figure 1 include ionomers neutralized with alkali, alkaline, and transition metals. Upon fitting the X-ray scattering data, an increase in both  $R_1$  and  $R_{CA}$  as a function of increasing neutralizing ionic radii is observed (Figure 4).  $R_1$  increases 55% as the ionic radii more than doubles from Cu

(0.71 Å) to Cs (1.65 Å). The increase in ionic aggregate size ( $R_1$ ) with cation size is independent of valence: monovalent (Na, Cs), divalent (Cu, Mg, Zn, Ba). The interpretation of this increase in  $R_1$  is complicated by the fact that the number of cations per aggregate is not constant in these P(S-SS<sub>x</sub>) ionomers, as described below.

The fitting parameters from the X-ray model are used to calculate the number of cations in an ionic aggregate ( $N_{agg}$ ) using two methods. In the first method, the volume of an ionic aggregate is divided by the estimated volume of an ionic group to give the number of cations in an ionic aggregate,  $N_{agg}(R_1)$ . This method assumes the ionic aggregates are exclusively composed of ionic groups, as proposed by Eisenberg, Hird, and Moore.<sup>23</sup> The second method uses the average composition of the ionomer to determine the number of ion pairs within a volume of  $V_p$  where there is on average a single ionic aggregate,  $N_{agg}(V_p)$ . This calculation also assumes that all of the ionic groups are in the ionic aggregates.

Using the first method,  $N_{agg}(R_1)$  for P(S-SS<sub>0.019</sub>) neutralized with monovalent cations is calculated by using a coordination structure for each acid–counterion group similar to the metal sulfate. The volume ( $V_{acid-ion}$ ) occupied by an acid–counterion pair (e.g.,  $\text{Na}^+\text{SO}_3^-$ ) is estimated using the density ( $\rho_{sulfate}$ ) and the molar mass ( $M_{sulfate}$ ) of anhydrous metal sulfate that corresponds to the specific neutralizing cation, coupled with the number of atoms in the acid–counterion pair ( $1\text{Na} + 1\text{S} + 3\text{O} = 5$ ), relative to the total number of atoms in the metal sulfate salt ( $2\text{Na} + 1\text{S} + 4\text{O} = 7$ ). For P(S-SS<sub>0.019</sub>) neutralized with divalent cations, the number of atoms in the acid–counterion pair (e.g.,  $\text{Cu}^{2+}(\text{SO}_3^-)_2$ ) is 9 ( $1\text{Cu} + 2\text{S} + 6\text{O}$ ) in comparison to the 6 total number of atoms in the metal sulfate salt ( $1\text{Cu} + 1\text{S} + 4\text{O}$ ).  $V_{acid-ion}$  ranges from 0.06 to 0.11 nm<sup>3</sup> for monovalent and divalent neutralized P(S-SS<sub>0.019</sub>). This estimation method of  $V_{acid-ion}$  has been applied previously.<sup>6</sup> The number of cations per ionic aggregate  $N_{agg}(R_1)$  is simply the volume ratio of an ionic aggregate relative to an acid–ion pair, with the implied assumption that the ionic aggregate is solely composed of ionic materials.

$$N_{agg}(R_1) = \frac{\frac{4}{3}\pi R_1^3}{V_{acid-ion}} \quad (7)$$

Alternatively, the number of cations per ionic aggregates can be determined by the number of acid–counterion groups present in a volume of  $V_p$ , which is the sample volume per aggregate. This method also assumes that all the available cations reside in the ionic aggregates.

$$N_{agg}(V_p) = \phi_{SS} V_p \eta_{SS} \quad \text{monovalent cations} \quad (8)$$

$$N_{agg}(V_p) = \frac{1}{2} \phi_{SS} V_p \eta_{SS} \quad \text{divalent cations} \quad (9)$$

The volume fraction of acid groups ( $\phi_{SS}$ ) is estimated using densities and molar mass of polystyrene ( $\rho_{PS} = 1.05 \times 10^{-21}$  g/nm<sup>3</sup> and  $M_{PS} = 104$  g/mol) and poly(styrenesulfonate) ( $\rho_{SS} = 1.43 \times 10^{-21}$  g/nm<sup>3</sup> and  $M_{SS} = 184$  g/mol). The number of styrenesulfonates per unit volume ( $\eta_{SS}$ ) depends on the copolymer composition in fully neutralized ionomers, so for all these P(S-SS<sub>0.019</sub>)-M ionomers  $\eta_{SS}$  is 4.7.

The  $N_{agg}(R_1)$  and  $N_{agg}(V_p)$  of the monovalent and divalent neutralized P(S-SS<sub>0.019</sub>) ionomers are compared in Figure 5. The  $N_{agg}(R_1)$  and  $N_{agg}(V_p)$  values are consistent for each ionomer, resulting in an occupancy ratio,  $N_{agg}(V_p)/N_{agg}(R_1)$ , that is approximately one. An occupancy ratio equal to one suggests that the ionic aggregate is composed solely of ionic species, and the surrounding matrix is free of ionic groups. In contrast, an occupancy ratio smaller than one indicates an insufficient number of cations available in  $V_p$  to fill an ionic aggregate of

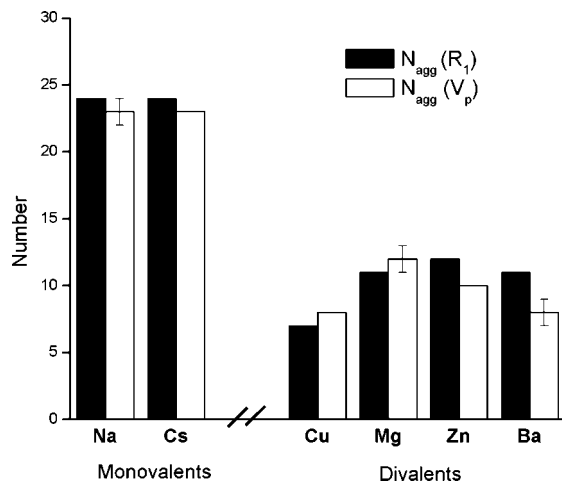


**Figure 5.** Comparison of the number of cations per ionic aggregate as calculated from  $R_1$  using eq 7 and  $V_P$  using eq 8 or eq 9 for P(S-SS<sub>0.019</sub>) ionomers neutralized with various cations. Error bar represent the uncertainty associated with determining  $V_P$ .

**Table 2. Fitting Parameters from the Kinning–Thomas Model of Fully Neutralized Styrene-Based Ionomers along with the Estimated Number of Cations in the Ionic Aggregates**

	P(S-SS <sub>0.070</sub> )-Cu	P(S-MAA <sub>0.072</sub> )-Cu
$R_1$ (nm)	0.83	0.60
$R_{CA}$ (nm)	1.56	0.69
$V_P$ (nm <sup>3</sup> )	60 ± 2	6.4 ± 0.4
$N_{agg}(R_1)$	32	12
$N_{agg}(V_P)$	12–14	1–2
$N_{agg}(V_P)/N_{agg}(R_1)$	~0.4	~0.1

size  $R_1$ . Therefore, this implies the presence of nonionic species and ionic groups in the aggregates. Alternatively, an occupancy ratio of greater than one implies that there are ions distributed through the matrix.

Another distinctive feature from Figure 5 is that both  $N_{agg}(R_1)$  and  $N_{agg}(V_P)$  values are consistently higher for the monovalent cations as compared to the divalent cations. In fact, the number of cations per aggregate is ~2–3 times higher for monovalent cations relative to divalent cations. In contrast, Figure 4 shows no distinction with valence as  $R_1$  and  $R_{CA}$  increase with atomic radii. These results combine to indicate that the cation concentration with monovalent counterions is considerably denser than with divalent counterions and the ionic radii is secondary.

**Comparison of Two Styrenic Ionomers.** Finally, we compare P(S-SS<sub>0.070</sub>) and P(S-MAA<sub>0.072</sub>) ionomers that have both been fully neutralized with copper in solution and solvent cast. Although quite similar these two ionomers have important differences: (1) sulfonic acids are stronger and larger than carboxylic acids and (2) the sulfonic acids are attached to the *para*-position of the phenyl groups while the carboxylic acids are directly attached to the carbon backbone. X-ray scattering results for P(S-SS<sub>0.070</sub>)-Cu and P(S-MAA<sub>0.072</sub>)-Cu show that  $R_1$ ,  $R_{CA}$ , and  $V_P$  are larger for P(S-SS<sub>0.070</sub>)-Cu by 38%, 126%, and 838%, respectively (Table 2).

Regions of limited polymer mobility surround each ionic aggregate and have a thickness of ( $R_{CA} - R_1$ ). These limited mobility regions cannot interpenetrate and thereby determine the minimum center-to-center distance between the ionic aggregates. The ( $R_{CA} - R_1$ ) values are 0.73 and 0.09 nm for P(S-SS<sub>0.070</sub>)-Cu and P(S-MAA<sub>0.072</sub>)-Cu, respectively. The much thicker region of limited mobility found in P(S-SS<sub>0.070</sub>)-Cu is consistent with having the acid group attached to the backbone via a phenyl ring rather than directly attaching to the polymer backbone as in P(S-MAA<sub>0.072</sub>)-Cu (Figure 6).

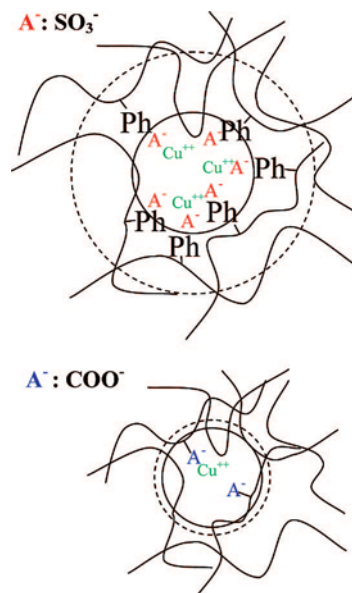


**Figure 6.** Schematic representing the X-ray scattering results for ionic aggregates in (a) P(S-SS<sub>0.070</sub>)-Cu and (b) P(S-MAA<sub>0.072</sub>)-Cu, where the solid circle is the cation-rich region of radius  $R_1$ . The dashed circle represents the radius of closest approach area of  $R_{CA}$ . Only a portion of the polymers is shown. Ph and A denote the phenyl group and acid groups, respectively. See the Supporting Information for the results from the Kinning–Thomas scattering model.

The number of cations per ionic aggregate was calculated as above using the aggregate size and the ionomer composition to give  $N_{agg}(R_1)$  and  $N_{agg}(V_P)$ . The P(S-MAA<sub>0.072</sub>)-Cu ionomer has  $N_{agg}(R_1) = 12$  and  $N_{agg}(V_P) = 1–2$  to give an occupancy ratio of only ~0.1. Other studies of P(S-MAA<sub>x</sub>)-M ionomers have found similarly small occupancy ratios, indicating that the ionic aggregates contain significant amounts of nonionic species.<sup>6</sup> The P(S-SS<sub>0.070</sub>)-Cu ionomer has  $N_{agg}(R_1) = 32$  and  $N_{agg}(V_P) = 12–14$  to give an occupancy ratio of ~0.4. This indicates that the P(S-SS<sub>0.070</sub>)-Cu ionomer has more ionic species within the ionic aggregate than P(S-MAA<sub>0.072</sub>)-Cu. Overall, the higher ionic content in ionic aggregates found in P(S-SS<sub>x</sub>)-Cu is the result of sulfonic acid being a stronger acid than carboxylic acid. Note, in addition, that the lower acid P(S-SS<sub>0.019</sub>)-Cu ionomer has an even higher occupancy ratio (~1), implying ionic aggregates are composed exclusively of ion pairs (Figure 5). Furthermore,  $N_{agg}(R_1)$  and  $N_{agg}(V_P)$  for P(S-SS<sub>0.019</sub>)-Cu are smaller for the lower acid level (~7). Thus, within the P(S-SS<sub>x</sub>)-Cu ionomers increasing the acid content leads to larger ionic aggregates with more cations but overall less ionic content in the ionic aggregates.

One implication of higher ionic content in the ionic aggregates of P(S-SS<sub>x</sub>) ionomers is that the number density ( $1/V_P$ ) of ionic aggregates is smaller at fixed acid level. This implies a lower rubbery plateau modulus because the ionic aggregates behave as physical cross-links. Viscoelastic data from by Hird and Eisenberg compared P(S-SS<sub>0.11</sub>)-Na and P(S-MAA<sub>0.107</sub>)-Na, and show that the modulus of the rubbery plateau in P(S-SS<sub>0.11</sub>)-Na is lower than the complementary ionomer with a carboxylic acid.<sup>25</sup> Similarly, our study finds that P(S-SS<sub>0.070</sub>)-Cu has a smaller aggregate number density than P(S-MAA<sub>0.072</sub>)-Cu.

A second implication of a higher ionic content is that the ionic aggregates are expected to be mechanically more robust, such that the physical cross-links persist to higher temperatures and are stronger. Hird and Eisenberg found that the viscoelastic rubbery plateau extends to higher temperatures in P(S-SS<sub>0.11</sub>)-Na than in either P(S-MAA<sub>0.107</sub>)-Na or poly(styrene carboxylate<sub>0.099</sub>)-Na.<sup>25</sup> Lundberg and Makowski performed viscosity measurements on P(S-SS<sub>x</sub>)-Na and poly(styrene carboxylate)-

Na containing 0.3–5.0 mol % ionic functionality and found that the sulfonated polystyrenes have a melt viscosity that is 3 orders of magnitude higher.<sup>26</sup> These examples clearly demonstrate that the P(S-SS<sub>x</sub>) ionomers possess stronger ionic aggregates because the stronger sulfonic acid produces ionic aggregates that contain a higher fraction of ionic species (larger occupancy ratio,  $N_{\text{agg}}(R_1)/N_{\text{agg}}(V_P)$ ) as compared to ionomers with carboxylic acids.

## Conclusions

This paper reports the first quantitative reconciliation of imaging and scattering data that details the nanoscale morphology of ionic aggregates in P(S-SS<sub>x</sub>) ionomers. We examined the morphology of solvent-cast and spin-cast P(S-SS<sub>0.019</sub>)-M ionomers using the combination of direct STEM imaging and X-ray scattering. The scattering data were fit with a liquidlike hard-sphere model proposed by Kinning and Thomas and give ionic aggregate sizes ( $R_1$ ) that are in good agreement with the STEM. The sample volume per ionic aggregate ( $V_P$ ) is also in good agreement between X-ray scattering and STEM imaging after the extensive particle overlap was accounted for via our previously published image simulation method.

STEM found that P(S-SS<sub>0.019</sub>) ionomers prepared by spin-casting exhibit nanometer spherical ionic aggregates that are indistinguishable in size, shape, and spatial distribution from the bulk solvent-cast ionomers. More work is necessary to determine the extent to which this finding can be generalized. In this specific class of ionomers, our previously published results for homopolymer–ionomer blend miscibilities using thin spin-cast films are likely to be applicable to bulk systems. Moreover, spin-cast films offer a number of practical advantages in preparing STEM specimens of these ionomers.

Six P(S-SS<sub>0.019</sub>)-M ionomers fully neutralized with various cations have ionic aggregate compositions that are predominately ionic. When P(S-SS<sub>0.019</sub>) is neutralized with a monovalent cation, the ionic aggregates have 2–3 times the number of cations per aggregate as compared to ionomers neutralized with divalent cations. However, independent of valency, the ionic aggregate radius ( $R_1$ ) and the radius of closest approach ( $R_{CA}$ ) in these ionomers increase as the cation radii increases. Overall, these results indicate that the cation concentration in the ionic aggregates is considerably higher for monovalent cations.

Finally, the influence of copolymer type was studied by comparing P(S-SS<sub>0.070</sub>) and P(S-MAA<sub>0.072</sub>) ionomers. The region of limited mobility is larger for the sulfonic acid ionomer, which correlates to having the acid group attached to a phenyl ring. Also, as expected for a stronger acid, the ionic aggregates in the P(S-SS<sub>0.070</sub>)-Cu ionomer are more ionic while those in the P(S-MAA<sub>0.072</sub>)-Cu ionomer incorporate a considerable amount of nonionic species.

The reconciliation of STEM and X-ray scattering in these P(S-SS<sub>x</sub>) ionomers has fueled our drive to extract detailed morphological information from the scattering data, particularly regarding the composition of the ionic aggregates, which is relevant for the mechanisms of ion transport. Although STEM and X-ray scattering have been reconciled for the P(S-SS<sub>x</sub>) ionomers studied here, a broad application of the liquidlike hard-sphere scattering model is not recommended. The specific interactions in these ionomers require that each new preparation method and ionomer type be studied with STEM to determine

whether or not a liquidlike arrangement of monodisperse spherical ionic aggregates is an appropriate structural model. For example, the STEM and X-ray scattering results from polyethylene-based ionomers have not yet been reconciled.

**Acknowledgment.** The authors thank Dr. Paul Heiney for adding the liquidlike X-ray model with the Percus–Yevick correlation function proposed by Kinning and Thomas functionality into the Datasqueeze software. Financial support for this work was provided by the U.S. Army Research Office (DAAD19-03-1-0130), NSF-IGERT Graduate Fellowship (DGE-0221664), and NSF-DMR (05-49116).

**Supporting Information Available:** Comparison of the Yarusso–Cooper and the Kinning–Thomas scattering models on styrenic ionomers; scattering data and fitting parameters for P(S-SS<sub>0.070</sub>)-Cu and P(S-MAA<sub>0.072</sub>)-Cu ionomers. This material is available free of charge via the Internet at <http://pubs.acs.org>.

## References and Notes

- (1) Eisenberg, A.; Kim, J.-S. *Introduction to Ionomers*; John Wiley & Sons: New York, 1998; p 352.
- (2) Elabd, Y. A.; Napadensky, E.; Sloan, J. M.; Crawford, D. M.; Walker, C. W. *J. Membr. Sci.* **2003**, *217*, 227–242.
- (3) Yarusso, D.; Cooper, S. L. *Macromolecules* **1983**, *16*, 1871–1880.
- (4) Benetatos, N. M.; Smith, B. W.; Heiney, P. A.; Winey, K. I. *Macromolecules* **2005**, *38*, 9251–9257.
- (5) Benetatos, N. M.; Heiney, P. A.; Winey, K. I. *Macromolecules* **2006**, *39*, 5174–5176.
- (6) Benetatos, N. M.; Chan, C. D.; Winey, K. I. *Macromolecules* **2007**, *40*, 1081–1088.
- (7) Kirkmeyer, B. P.; Taubert, A.; Kim, J.-S.; Winey, K. I. *Macromolecules* **2002**, *35*, 2648–2653.
- (8) Kirkmeyer, B. P.; Weiss, R. A.; Winey, K. I. *J. Polym. Sci., Part B: Polym. Phys.* **2001**, *39*, 477–483.
- (9) Register, R. A.; Sen, A.; Weiss, R. A.; Cooper, S. L. *Macromolecules* **1989**, *22*, 2224–2229.
- (10) O'Connell, E. M.; Root, T. W.; Cooper, S. L. *Macromolecules* **1995**, *28*, 3995–3999.
- (11) Zhou, N. C.; Xu, C.; Burghardt, W. R.; Composto, R. J.; Winey, K. I. *Macromolecules* **2006**, *39*, 2373–2379.
- (12) Yarusso, D.; Cooper, S. L. *Polymer* **1985**, *26*, 371–378.
- (13) Fitzgerald, J. J.; Weiss, R. A. *J. Macromol. Sci., Rev. Macromol. Chem. Phys.* **1988**, *C28*, 99–185.
- (14) Dickinson, L. C.; Weiss, R. A.; Wnek, G. E. *Macromolecules* **2001**, *34*, 3108–3110.
- (15) Kinning, D. J.; Thomas, E. L. *Macromolecules* **1984**, *17*, 1712–1718.
- (16) Heiney, P. A. *Comm. Powder Diffr. Newsletter* **2005**, *32*, 9–11.
- (17) Benetatos, N. M.; Winey, K. I. *Macromolecules* **2007**, *40*, 3223–3228.
- (18) Batra, A.; Cohen, C.; Kim, H.; Winey, K. I.; Ando, N.; Gruner, S. M. *Macromolecules* **2006**, *39*, 1630–1638.
- (19) Carvalho, A. J. F.; Curvelo, A. A. S. *Macromolecules* **2003**, *36*, 5304–5310.
- (20) Baigl, D.; Seery, T. A. P.; Williams, C. E. *Macromolecules* **2002**, *35*, 2318–2326.
- (21) Register, R. A.; Bell, T. R. *J. Polym. Sci., Part B: Polym. Phys.* **1992**, *30*, 569–575.
- (22) Zhou, N. C.; Winey, K. I. Ph.D. Dissertation, University of Pennsylvania, 2007.
- (23) Eisenberg, A.; Hird, B.; Moore, R. B. *Macromolecules* **1990**, *23*, 4098–4107.
- (24) Zhou, N. C.; Burghardt, W. R.; Winey, K. I. *Macromolecules* **2007**, *40*, 6401–6405.
- (25) Hird, B.; Eisenberg, A. *Macromolecules* **1992**, *25*, 6466–6474.
- (26) Lundberg, R. D.; Makowski, H. S. *Abstr. Pap. Am. Chem. Soc.* **1978**, *176* (SEP), 85–85.

MA800805M